J Low Temp Phys (2013) 171:606–612
DOI 10.1007/s10909-012-0790-5

Phase Diagrams of ^{4}He on Flat and Curved Environments

M.C. Gordillo · J. Boronat

Received: 4 July 2012 / Accepted: 10 October 2012 / Published online: 23 October 2012

Abstract By means of diffusion Monte Carlo calculations, we obtained the phase diagrams of a first and second layer of ^{4}He on graphene and on the outside of different isolated armchair carbon nanotubes with radii in the range 3.42 to 10.85 Å. That corresponds to tubes between the (5, 5) and (16, 16) in standard nomenclature. In both cases, the ground state is either a liquid (second layer on graphene and on nanotubes whose radii is greater than ∼7 Å) or an incommensurate solid (for thinner tubes). In the former case, upon a density increase, the system undergoes a first-order phase transition to another incommensurate solid. A study of the influence of the C–He potential (isotropic or anisotropic) on the phase diagrams is also presented.

Keywords Phase transitions · Helium

1 Introduction

Adsorption of gases such as ^{4}He and *para*-H_2 on carbon surfaces like graphite at very low temperatures are typical examples of reduced dimensionality quantum systems [1–3]. Their corresponding phase diagrams are quite rich since one can observe stable commensurate solids of different type, liquid layers and incommensurate solids [4]. With the technological progress in the generation of new carbon structures a

M.C. Gordillo (✉)
Departamento de Sistemas Físicos, Químicos y Naturales, Universidad Pablo de Olavide, Carretera de Utrera km 1, 41013 Sevilla, Spain
e-mail: cgorbar@upo.es

J. Boronat
Departament de Física i Enginyeria Nuclear, Universitat Politècnica de Catalunya, Campus Nord B4-B5, 08034 Barcelona, Spain
e-mail: jordi.boronat@upc.edu

fascinating plethora of arrangements are now available for adsorption: nearly spherical surfaces (fullerenes) [5], single-atom structures with two flat adsorption surfaces (graphene) [1–3], a modified flat surface (graphane) [6], and cylindrical setups with both inside and outside adsorption (nanotubes) [7].

Quantum Monte Carlo methods have been recently applied to the theoretical study of adsorption of quantum gases on these new carbon structures, both at zero temperature by means of the diffusion Monte Carlo (DMC) method [1, 2] and at finite temperature using path integral Monte Carlo (PIMC) [3]. Unfortunately, we cannot compare these results with experimental data yet, but the accuracy achieved in the reproduction of the experimental phase diagram on ^{4}He on graphite using the same methodology gives us confidence on the quality of the results obtained so far. The main uncertainties in these microscopic approaches derive from the possible deficiencies in the adsorbate atom-surface interaction. In the first studies [8–10, 12] it was usual to work with a smoothed interaction that depends only on the distance of the atom to the carbon plane. However, this potential is not able to generate a satisfactory phase diagram because no corrugation is present. Instead, in more recent simulations an explicit account of the sum of all the carbon-helium interactions has been included [1, 17, 18], making the resulting phase diagrams agree with available experimental data on graphite. In the present work, we further analyze the influence of the C–He interaction in the phase diagram by comparing the results obtained with two different potential models: an isotropic Lennard-Jones potential, used extensively in previous studies [13], and the anisotropic interaction proposed by Carlos and Cole to obtain a better agreement with certain experimental measurements [14].

In the next section, we briefly introduce the theoretical method used in our analysis and discuss the two pair potentials, isotropic and anisotropic. Section 3 contains the results obtained for the two interactions and in three different systems: the first and second layers of ^{4}He on graphene and the first layer of ^{4}He adsorbed on the external surface of a nanotube. Finally, the main conclusions are discussed in Sect. 4.

2 Method

The role of corrugation in the physical properties of adsorbed ^{4}He on carbon surfaces is analyzed by using the diffusion Monte Carlo (DMC) method. The DMC algorithm is nowadays a standard tool that provides exact results when solving the N-body Schrödinger equation for boson systems within some statistical errors. It does so by the introduction of an importance sampling strategy through a guiding wave function Ψ [15]. For the liquid phases studied in this work we have used

$$\Psi_L(\mathbf{r}_1, \mathbf{r}_2, \ldots, \mathbf{r}_N) = \prod_{i<j} \exp\left[-\frac{1}{2}\left(\frac{b}{r_{ij}}\right)^5\right] \prod_i \Phi(\mathbf{r}_i), \tag{1}$$

where the first part is a Jastrow wave function that depends on the distances r_{ij} between each pair of ^{4}He atoms. The one-body term $\Phi(\mathbf{r}_i)$ is a variational wave function describing the adsorption of a single atom on the carbon surface.

The solid phases are simulated with the help of a Nosanow-Jastrow wave function. In this case, Ψ is the product of Ψ_L (1) and of Gaussian terms that confine the ^{4}He

atoms around the crystallographic positions (x_I, y_I) of the two-dimensional solid arrangements we are interested in,

$$\Psi_S(\mathbf{r}_1, \mathbf{r}_2, \ldots, \mathbf{r}_N) = \Psi_L \prod_{i,I=1}^{N} \exp\{-c[(x_i - x_I)^2 + (y_i - y_I)^2]\}. \tag{2}$$

For the tube case, the confining takes place in all three dimensions, i.e., we have to add $(z_i - z_I)^2$ to the exponential above. The variational parameters entering Eqs. (1), (2) are optimized for the different studied geometries by preliminary variational Monte Carlo calculations.

In addition to the geometry of the system, phase, and atomic mass one needs to include accurate models for the interatomic potentials that appear in the Hamiltonian. The helium-helium interaction is accurately described by the semi-empirical Aziz potentials [16]. The interaction between ^{4}He and the adsorbing surface is rather well known but not with the accuracy nowadays achieved for the He–He potential. In the first studies of adsorption on graphite [8, 12], a smoothed interaction that approached the C–He pair interaction sum was used. However, more recent studies [1, 11, 18] substitute this integrated potential by explicit pair sums that, in practice, can be tabulated in a grid for an efficient use in the simulation. In this way, one recovers the experimental ground state and describes accurately the full experimental phase diagram [4]. In previous work [1, 2], we have built the potential surfaces using an isotropic Lennard-Jones potential with parameters used in studies of ^{4}He adsorbed inside narrow nanotubes [13]. In spite of the fact that the phase diagram seems correctly described by central interactions it has been claimed that the corrugation produced by this model is incomplete. In order to better account for some effects which are more sensitive to corrugation, Carlos and Cole [14] proposed an anisotropic pair interaction that incorporates the dielectric anisotropy of the graphite substrate,

$$V(\mathbf{r}) = 4\varepsilon\left\{\left(\frac{\sigma}{r}\right)^{12}\left[1 + \gamma_R\left(1 - \frac{6}{5}\cos^2\theta\right)\right] - \left(\frac{\sigma}{r}\right)^{6}\left[1 + \gamma_A\left(1 - \frac{3}{2}\cos^2\theta\right)\right]\right\}, \tag{3}$$

where θ is the angle between the surface normal and the vector distance $\mathbf{r}$ is between the ^{4}He atom and a particular C atom in the surface. The θ dependence of this potential (3) makes it deeper in the center of the carbon hexagons than in its sides, producing an increase of the corrugation effects.

3 Results

In Fig. 1, we show the equations of state of the different phases of a first layer of ^{4}He on graphene. There, we displayed two sets of similar symbols. The upper ones correspond to simulation results obtained by using the isotopic form of the C–He potential [13], while the lower symbols display the energies per particle derived from the use of the anisotropic potential [14]. We observe that both sets of data are very similar. For instance, for both potentials the ground state correspond to a $\sqrt{3} \times \sqrt{3}$

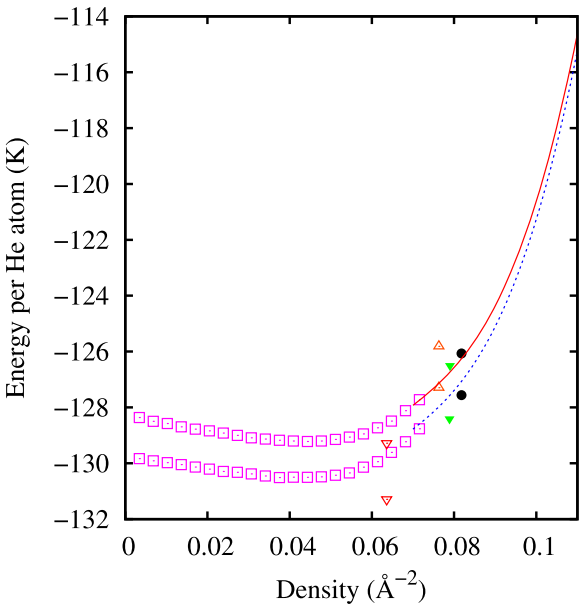

Fig. 1 Energy per particle for different phases of a first layer of helium on graphene: liquid, (*open squares*); $\sqrt{3} \times \sqrt{3}$, (*down open triangles*); 2/5 phase, (*open upper triangles*); 31/75 solid, (*full down triangles*); 3/7 commensurate phase (*full circles*). In all cases, the *upper curve* or *symbol* was obtained using the C–He isotopic potential and the *lower curve* is the corresponding to the anisotropic potential. The *solid curves* are third order polynomial fits to the simulation results for the a triangular incommensurate phase. (Color figure online)

commensurate structure. However, the energy stabilization of the solid is boosted in the case of the anisotropic interaction. The density at which the energy per particle is lowest in a liquid arrangement in the last case is 0.0416 ± 0.0004 Å^{-2} and corresponds to -130.53 ± 0.01 K. The energy per particle for the $\sqrt{3} \times \sqrt{3}$ structure is -131.29 ± 0.02 K. This means that the difference between them is -0.76 K vs. -0.061 K for the isotropic potential [1]. We also observe that when the C–He potential is the anisotropic one that registered solid undergoes a phase transition to a 31/75 structure upon a density increase (full down triangles in Fig. 1, energy per particle below that of an incommensurate structure at the same density) and after that to a 3/7 commensurate solid (full circles in the same figure). A further compression takes the system to a triangular incommensurate structure from 0.088 Å^{-2} up. This is at odds to what happens when the same phase diagram is calculated with an isotropic substrate-helium interaction. There, the transition is directly from a $\sqrt{3} \times \sqrt{3}$ solid to an incommensurate structure of density 0.08 Å^{-2}.

It is worth mentioning that a recent PIMC simulation of the first ^{4}He layer on graphene at finite temperature [3] showed different results on the superfluidity of the registered $\sqrt{3} \times \sqrt{3}$ phase depending on the pair interaction. In particular, Ref. [3] predicts the suppression of superfluidity in this commensurate solid with vacancies when the anisotropic interaction is used instead of the isotropic one. We have investigated this effect using DMC, and contrarily to what obtained in Ref. [3], we do not observe any significant difference when one potential is substituted by the other: our results with the anisotropic interaction are the same than the ones reported in Ref. [17].

If instead of considering the phase diagram for the helium layer closest to graphene, we consider what happens to a second helium sheet on top of it, one expects the influence of the particular C–He interaction to be greatly reduced. This is

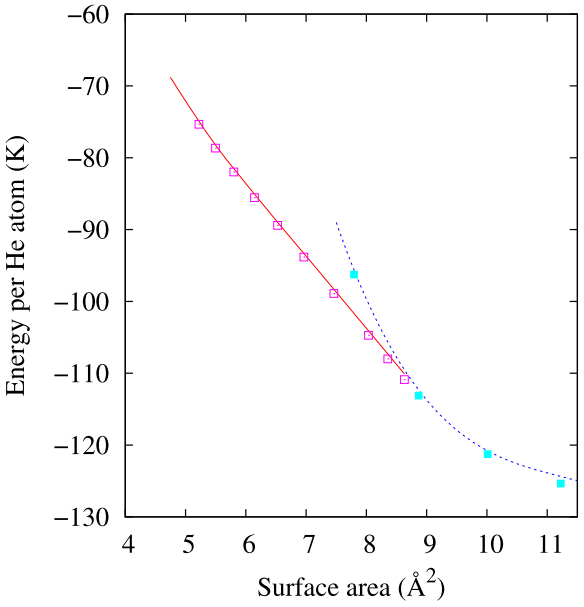

Fig. 2 Energy per particle obtained with an isotropic C–He interaction for single layer triangular solids of different densities (*dashed line*) and for systems made of a first layer solid of fixed density 0.115 Å^{-2} and second layer liquids with a variable number of particles. The respective *full* and *open symbols* represent the simulation results for the same arrangements using the anisotropic C–He interaction. (Color figure online)

basically due to the overall reduction of the C–He interaction for atoms on the second layer. This is exactly what we can see in Fig. 2. There, we display the energy per particle in the case of a first solid ^{4}He layer and a second liquid layer of helium on top of a triangular solid whose density is the adequate to minimize the total energy per particle of the entire arrangement (0.115 Å^{-2}). What we see is that when the helium density increases, the effect of the anisotropy in the C–He interaction decreases, both in the first and second layers. This can also be seen in the high density end of Fig. 1. In any case, the small differences in the energy per particle for both potentials play no role in the promotion density to the second layer (0.113 ± 0.001 Å^{-2}) or to the beginning of the formation to a second layer liquid (0.163 ± 0.005 Å^{-2}) [19]. These limit densities were obtained from a double-tangent Maxwell construction and compare favorably with the experimental ones on graphite [20, 21].

If the underlying carbon surface is curved, as in the case of carbon nanotubes, the phase diagram of helium changes with respect to graphene. In Fig. 3, we see the example of the case of a (10, 10) nanotube, to be compared with Fig. 1. There, the full circles correspond to the wrapped up version of a $\sqrt{3} \times \sqrt{3}$ structure, and both in the isotropic (lower set of symbols) and anisotropic (upper set of symbols) cases their energies are higher than the liquid energies at the same density. In the isotropic case, we can see also that the minimum energy per particle for the liquid (open squares) and incommensurate solid (full squares, a phase formed by rings of helium atoms whose plane is perpendicular to the main axis of the tube) are similar to each other. In fact, as it can be seen in Table 1, both energies are within each other error bars. However, for tubes whose radius is lower than the corresponding to a (10, 10) one, the lowest energy per particle correspond to an incommensurate solid (the (8, 8) case is displayed as an example). On the other hand, the opposite happens for wider radii, of which the (12, 12) is chosen as a representative. In that last case, the ground state

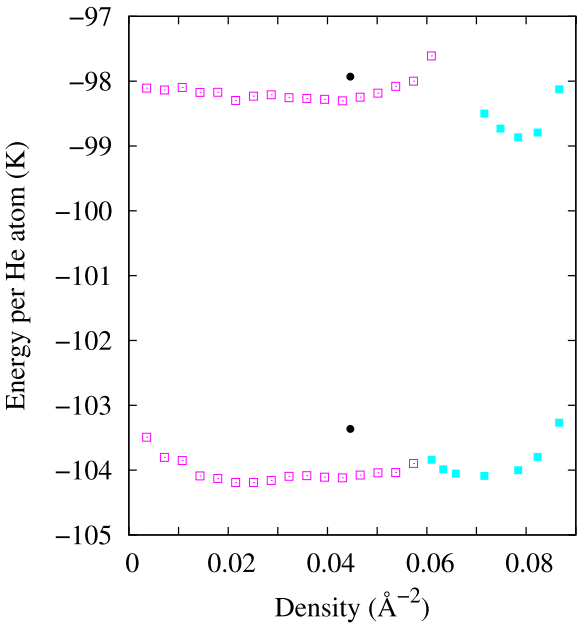

Fig. 3 Single layer liquid (*open squares*) and incommensurate solid phases (*full squares*) of helium on the outer surface on a (10, 10) tube. *Upper symbols*: anisotropic potential; *lower set of symbols*, isotropic potential. The *full circles* correspond to the wrapped equivalent of the $\sqrt{3} \times \sqrt{3}$ commensurate solid that is the ground state of ^{4}He on graphene. (Color figure online)

Table 1 Energies per particle (e_g) and equilibrium ^{4}He densities (ρ_g) for liquid helium phases for different tubes. The error bars affect to the last figure shown and are given in parenthesis. When the ground state is an incommensurate solid, the density for which the energy per particle is minimum is given as ρ_l. If the ground state is a liquid, the lowest density for which the incommensurate solid is stable, obtained from a Maxwell construction is given instead and is also displayed under the ρ_l column. ρ_u is the upper helium density for which the liquid is stable for the tube whose ground state is a liquid

Tube	radius (Å)	ρ_g (Å^{-2})	e_g (K)	ρ_u (Å^{-2})	e_u (K)	ρ_l (Å^{-2})	e_l (K)
(8, 8)	5.45	0.0358(1)	−102.02(2)	–	–	0.0744(9)	−102.50(2)
(10, 10)	6.8	0.0323(9)	−104.20(2)	–	–	0.0730(7)	−104.15(4)
(12, 12)	8.14	0.0241(9)	−105.40(2)	0.040(1)	−105.28(1)	0.067(1)	−105.05(2)

of helium on a carbon nanotube will be a liquid, whose upper stability limit is listed also in Table 1 as ρ_u. There, ρ_l means the lowest density for which the solid is stable. For a (16, 16) tube, the values are similar to those for the (12, 12) one [22].

All the results given in Table 1 are for an isotropic potential. In Fig. 3, we can see that for the (10, 10) tube, the use of an anisotropic potential has two main effects in the phase diagram: (i) the solid structure is stabilized with respect to the isotropic potential (this is exactly what happened with the graphene case discussed above), and (ii) the energy per particle increases with respect to the isotropic interaction. A similar calculation carried out for the (5, 5) cylinder, indicated that the solid stabilization is also seen in that tube for the anisotropic version of the potential. In that case, the energy per particle at for the incommensurate solid when the pressure equals zero goes from -96.10 ± 0.03 K (isotropic potential) to -87.76 ± 0.05 K (anisotropic one), from a density $\sim 0.061 \pm 0.01$ Å^{-2} in both cases.

4 Conclusions

We have carried out extensive diffusion Monte Carlo calculations to obtain the phase diagrams of ^{4}He adsorbed on different graphene surfaces. We found that both for a second layer of helium of graphene and for a first layer on the curved surface of a nanotube, the ground state is a liquid, providing that the carbon cylinder is big enough. Those results do not depend on the isotropic or anisotropic nature of the C–He pair interaction. However, when we used the Carlos and Cole [14] potential, we found that the first layer solids are stabilized with respect to a liquid phase. This is true both for the carbon nanotube case and for graphene.

Acknowledgements We acknowledge partial financial support from the Junta de Andalucía group PAI-205 and Grant FQM-5985, DGI (Spain) Grants FIS2010-18356 and FIS2011-25275, and Generalitat de Catalunya Grant 2009SGR-1003.

References

1. M.C. Gordillo, J. Boronat, Phys. Rev. Lett. **102**, 085303 (2009)
2. M.C. Gordillo, J. Boronat, Phys. Rev. B **81**, 155435 (2010)
3. Y. Kwon, D.M. Ceperley, Phys. Rev. B **85**, 224501 (2012)
4. L.W. Bruch, M.W. Cole, E. Zaremba, *Physical Adsorption: Forces and Phenomena* (Clarendon Press, Oxford, 1997)
5. E.S. Hernández, M.W. Cole, M. Boninsegni, Phys. Rev. B **68**, 125418 (2003)
6. L. Reatto, M. Nava, D.E. Galli, C. Billman, J.O. Sofo, M.W. Cole, arXiv:1204.3061v1 [cond-mat]
7. M.C. Gordillo, J. Boronat, J. Low Temp. Phys. **157**, 296 (2009). doi:10.1007/s10909-009-9912-0
8. P.A. Whitlock, G.V. Chester, B. Krishnamachari, Phys. Rev. B **58**, 804 (1998)
9. K. Nho, E. Manousakis, Phys. Rev. B **65**, 115409 (2002)
10. M.E. Pierce, E. Manousakis, Phys. Rev. B **62**, 5228 (2000)
11. M.E. Pierce, E. Manousakis, Phys. Rev. Lett. **83**, 5314 (1999)
12. M.C. Gordillo, D.M. Ceperley, Phys. Rev. B **58**, 6447 (1998)
13. G. Stan, M.W. Cole, Surf. Sci. **395**, 280 (1998)
14. W.E. Carlos, M.W. Cole, Surf. Sci. **91**, 339 (1980)
15. J. Boronat, J. Casulleras, Phys. Rev. B **49**, 8920 (1994)
16. R.A. Aziz, F.R.W McCourt, C.C.K. Wong, Mol. Phys. **61**, 1487 (1987)
17. M.C. Gordillo, C. Cazorla, J. Boronat, Phys. Rev. B **83**, 121406(R) (2011)
18. P. Corboz, M. Boninsegni, L. Pollet, M. Troyer, Phys. Rev. B **78**, 245414 (2008)
19. M.C. Gordillo, J. Boronat, Phys. Rev. B **85**, 195457 (2012)
20. D.S. Greywall, Phys. Rev. B **47**, 309 (1993)
21. P.A. Crowell, J.D. Reppy, Phys. Rev. B **53**, 2701 (1996)
22. M.C. Gordillo, J. Boronat, submitted